AIAA JOURNAL
Vol. 32, No. 10, October 1994

Comparison of NO and OH Planar Fluorescence Temperature Measurements in Scramjet Model Flowfields

B. K. McMillin,* J. M. Seitzman,† and R. K. Hanson‡
Stanford University, Stanford, California 94305

The use of nitric oxide (NO) and the hydroxyl radical (OH) as temperature tracers, in a two-line planar laser-induced fluorescence technique, is examined in the context of a supersonic mixing and combustion flowfield. The temperature measurements were based on the sequential excitation of two transitions, either in the $A \leftarrow X$ (0,0) band of NO near 226 nm or the $A \leftarrow X$ (1,0) band of OH near 283 nm. The measurements were obtained for each species through the use of two lasers and two cameras, with each camera integrating signal induced from only one of the lasers. Both temporally resolved and frame-averaged temperature measurements of each species are presented. Additional results include simultaneous NO and OH visualizations, in which seeded NO marks the fuel jet fluid and nascent OH marks the reaction zones and convected combustion gases. A detailed temperature comparison shows good agreement in the common measurement regions and indicates that shot noise is the largest source of uncertainty. The comparison also illustrates the importance of a careful interpretation of the measurements, since, depending on the origin of the tracer and the degree of mixing, the measurements may be biased toward the fuel, freestream, or reaction zone temperatures.

Introduction

THE recent interest in the development of scramjet propulsion technology has motivated both experimental and computational studies aimed at increasing the understanding of supersonic mixing and combustion. A number of recent experimental studies have employed laser-based planar imaging techniques to examine these phenomena, because imaging techniques can provide both flow visualization and the opportunity for quantitative property measurements with high spatial and temporal resolution. For example, two-dimensional imaging techniques including Rayleigh/Mie scattering and planar laser-induced fluorescence (PLIF) have been applied in studies of compressible free shear layers[1–4] and transverse jets in supersonic crossflow,[5–9] to examine phenomena such as large-scale turbulent structures, compressibility effects, temperature fields, velocity fields, and the location of reaction zones.

In these types of flows, temperature measurements are of particular interest for examining fuel/air mixing (when the streams are at different temperatures), for monitoring heat release and its influence on the fluid mechanics, for locating reaction zones, and for studying the convective heat transfer to combustor walls. The purpose of this paper is to explore and compare the use of nitric oxide (NO) and the hydroxyl radical (OH) as temperature tracers in supersonic mixing and combustion flows, using the two-wavelength PLIF strategy.[10] Our focus is on NO and OH, since they are two of the most widely used diagnostic species in combustion flowfields, and on the two-line strategy, since it is the most versatile technique for complex supersonic flows, which typically have large variations in pressure and species' concentrations. Although a limited number of two-line PLIF temperature measurements of NO (Refs. 9 and 11–13) and OH (Refs. 14–17) have been reported, this is the first study where a direct comparison can be made, with both measurements obtained in the same complex flowfield.

In this paper, we briefly review the two-line temperature technique and discuss the advantages and limitations of each species as a temperature tracer, in the context of supersonic mixing and combustion flows. We then describe the scramjet model flowfield considered here and examine temporally resolved NO and OH visualizations, obtained essentially simultaneously, which show the spatial distributions of the fuel and combustion gases. To illustrate their complementary features, both temporally resolved and frame-averaged, NO and OH temperature measurements are then presented and compared. Finally, we discuss temperature interpretation considerations, since depending on the origin of the tracer and the degree of mixing, the measurements may be biased toward the fuel, freestream, or reaction zone temperatures.

Planar Laser-Induced Fluorescence Technique

Two-Line Temperature Strategy

As a molecular temperature diagnostic, PLIF measurements are typically based on probing the temperature-dependent population of one or more rotational states of a species present within the flow.[10] For a given measurement, the laser is tuned to excite a particular rovibronic transition (originating in the electronic ground state), and the resulting fluorescence is collected with an intensified, solid-state camera. The fluorescence signal is thus used as an indirect measure of absorption and depends on a number of properties including the absorbing species number density, the Boltzmann population fraction of the absorbing state, and the absorption and laser line shapes. Competing nonradiative decay processes cause the fluorescence to depend on various collisional transfer rates as well.

Several excitation strategies, including both one- and two-wavelength techniques, have been developed to determine the gas temperature from the fluorescence signal(s) in various situations.[10,18] The essence of the two-line technique employed here is to use the fluorescence ratio, obtained by sequentially exciting two different initial states of a particular gas species, to infer the temperature from the ratio of absorbing state populations. By taking the ratio of fluorescence signals, the signal dependence on the number density, absorbing species mole fraction, overlap integral, and collisional quenching can be minimized. Thus, the signal at each pixel within the ratio image (ideally) depends upon only the relative Boltzmann fractions of the states probed.

In this application, the rotational temperature is obtained by exciting transitions that originate from different rotational states

Presented as Paper 93-2035 at the AIAA/SAE/ASME/ASEE 29th Joint Propulsion Conference, Monterey, CA, June 28–30, 1993; received Aug. 6, 1993; revision received April 4, 1994; accepted for publication April 11, 1994.

*Postdoctoral Fellow; currently National Research Council NIST Postdoctoral Research Associate, Chemical Science and Technology Laboratory, National Institute of Standards and Technology, Gaithersburg, MD 20899. Member AIAA.

†Research Associate; currently Assistant Professor, School of Aerospace Engineering, Georgia Institute of Technology, Atlanta, GA 30332. Member AIAA.

‡Professor, High Temperature Gasdynamics Laboratory, Department of Mechanical Engineering. Senior Member AIAA.

within the same vibrational level of the electronic ground state. In the limit of weak excitation, the fluorescence ratio R_{12} can be modeled as[10]

$$R_{12} = C'_{12} \frac{B_1 E_1 f_{B1}(T)\, g_1(\chi_i, N, T)\, \phi_1(\chi_i, N, T)}{B_2 E_2 f_{B2}(T)\, g_2(\chi_i, N, T)\, \phi_2(\chi_i, N, T)} \quad (1)$$

where C'_{12} is a constant which depends on the detection systems, B the Einstein coefficient for stimulated absorption, E the laser pulse energy, g the overlap integral between the absorption and laser line shapes, N the gas density, T the gas kinetic/rotational temperature, and f_B the Boltzmann population fraction of the absorbing state. Also, ϕ is the fluorescence yield, which depends on the species mole fractions χ_i, the spontaneous emission (A), and collisional quenching rate coefficients (Q), and is given by $\phi = A/[A + Q(\chi_i, N, T)]$; and the subscripts 1 and 2 refer to the values associated with the respective fluorescence images. If we assume the primary temperature dependence results from the Boltzmann fractions and incorporate the various spectroscopic terms into C_{12}, the fluorescence ratio can be written as an explicit function of temperature, given by

$$R_{12} = C_{12} \frac{E_1}{E_2} \exp\left[-\frac{\Delta\varepsilon_{12}}{kT}\right] \quad (2)$$

where $\Delta\varepsilon_{12}$ is the energy difference between the initial absorbing states and k the Boltzmann constant. The constant C_{12} can be determined by independent calibration or from the signal ratio directly (in situ), if the temperature is accurately known at some location within the image.

Relating the fluorescence ratio to temperature solely through the population fraction simplifies the data analysis but creates potential sources of systematic errors: specifically, any temperature dependence of the ratios g_1/g_2 and ϕ_1/ϕ_2. For spectral broadening dominated by Doppler and simple collisional (Lorentzian-type) mechanisms, g_1/g_2 can vary with temperature if 1) the two transitions have significantly different center frequencies and, therefore, Doppler broadening, or 2) the collisional broadening is transition (i.e., rotational quantum number J) dependent. One advantage of the current rotational temperature measurements is that the selected transitions are within the same vibrational band and, thus, have similar center frequencies and Doppler broadening.

Similarly, the fluorescence yield ratio ϕ_1/ϕ_2 can show temperature dependence under three scenarios: 1) J-dependent spontaneous emission rates, 2) J-dependent quenching rates, and 3) nonnegligible fluorescence trapping (resonant absorption of the fluorescence by gas between the measurement plane and the detection system) which is different for the two images. Generally, if both images are collected through the same or equivalent optical paths, potential trapping effects are minimized in the ratio image.

Other potential sources of systematic error have been described previously.[9,15,17] In the current measurements, the most important are pulse-to-pulse differences in the calibration constant C_{12}, induced by shot-to-shot mode fluctuations in the lasers' spectral profiles.[9,17,19] When the calibration point is acquired from the image itself, however, this error is avoided. Additionally, nonlinear averaging of temperature variations on a scale smaller than the effective spatial resolution of the image can occur.[9,19]

NO and OH as Temperature Tracers

As noted earlier, NO and OH are two of the most widely used species for PLIF measurements in combustion flows. As a tracer for fluorescence imaging of reacting flows, NO has the advantages that it is relatively stable, easily seeded or naturally present (e.g., in high temperature air flows), and well-understood spectroscopically. Potential drawbacks of NO include its toxicity and its ability to sensitize ignition at low temperatures or high pressures[20]; however, neither is significant in the current flowfield. The OH radical is produced at easily measurable levels in most high temperature combustion flows and its spectroscopic behavior is also well characterized. Although OH is an equilibrium combustion product in this high speed flow, high (i.e., superequilibrium) concentrations of OH generally mark regions of reaction and, because of relatively slow recombination rates, regions containing hot convected combustion gases.

In this study, the NO fluorescence images were acquired by exciting transitions within the $A^2\Sigma^+ \leftarrow X^2\Pi\,(v'=0, v''=0)$ γ-band, near 226 nm. In this band, transitions from a large range of rotational levels are easily accessible with pulsed dye lasers. The (0,0) band also has relatively strong absorption, thereby providing high fluorescence signals, while allowing for efficient rejection of laser scattering through nonresonant detection of broadband fluorescence to vibrationally excited levels (primarily $v''>2$) (Ref. 19). With this nonresonant detection approach, fluorescence trapping is also minimized, since these excited vibrational levels are negligibly populated and produce little absorption in most combustion environments. NO temperature measurements should also be free of systematic errors associated with the ratios g_1/g_2 and ϕ_1/ϕ_2, since collisional broadening,[21] spontaneous emission rates,[22,23] and collisional quenching[22,24] have been shown to be rotation-level independent for this NO γ-band.

For quantitative OH imaging of the ground $v''=0$ state, various laser pumping schemes have been demonstrated. For single-shot imaging with good spatial resolution, dye laser excitation of the $A^2\Sigma^+ \leftarrow X^2\Pi$ (1,0) band near 283 nm combined with detection of the direct (1,1) and indirect, collision-induced (0,0) emission bands appears to be the best approach. It provides good signal-to-noise ratio measurements, reasonably low systematic errors, rejection of scattered light, and flexibility in choosing excitation transitions optimized for a specific flow condition.[25]

Unlike NO, OH does exhibit J-dependent collisional broadening, spontaneous emission, and quenching rates. At elevated temperatures, though, collision broadening has been shown to vary little for $J>5.5$ (Ref. 26), and similarly, the J dependence of the fluorescence yield (through A and Q) appears to be insignificant for temperatures above ~1000 K and $J>5.5$ (Ref. 17). Also unlike the NO technique, this OH excitation strategy is potentially susceptible to fluorescence trapping, since the $v'=1$–0 transfer rate is J-dependent,[27] and the indirectly produced (0,0) band emission can show significant absorption if large path lengths or high concentrations of OH are present[28]; however, as noted, potential temperature errors in the ratio image due to fluorescence trapping should be minimized if both cameras collect through the same optical path.

Experimental Details

Flow Facility/Planar Laser-Induced Fluorescence Systems

The flow facility and PLIF imaging systems used in these measurements have been described in detail previously[9,19] and are briefly reviewed here. Figure 1 shows a schematic of the facility. The flows were generated in a pressure-driven shock tube by injecting a gaseous fuel jet into the supersonic flow behind an incident shock wave. The test section has a 76×76-mm square cross section, and the fuel was injected through a pulsed solenoid valve with a 2-mm-diam orifice. The valve was triggered so that the jet

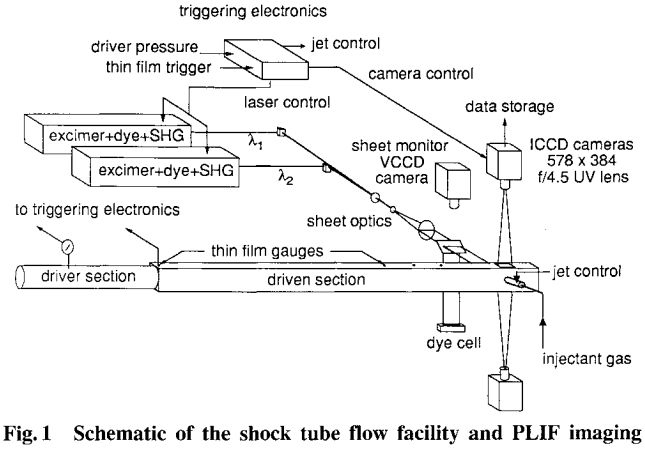

Fig. 1 Schematic of the shock tube flow facility and PLIF imaging systems.

flow reached steady state prior to the incident shock arrival, and the images were acquired ~200 μs after passage of the incident shock to provide (some) time for the plume to develop.

The frequency-doubled outputs of two XeCl excimer-pumped dye lasers were used as the excitation sources. Each laser had a pulse width of ~20 ns and a pulse energy at the test section of ~0.2–0.4 mJ, in a spectral bandwidth of ~0.3–0.4 cm^{-1}. The beams were formed into sheets (~300 μm×75 mm) using a cylindrical telescope and spherical lens. As indicated in the schematic, the beams were combined geometrically by propagating them at a slight vertical angle to one another. The beam heights and angles were adjusted so that the sheets crossed near the center of the imaged region, with no significant differences in the combined sheet thickness and position.

For the NO temperature measurements, the lasers were tuned to the $R_1+Q_{21}(13.5)$ and $Q_1+P_{21}(28.5)$ transition pairs. These transitions were selected to provide a reasonable temperature sensitivity ($\Delta\varepsilon_{12}/k \sim 1531$ K) within the plume ($T<1800$ K), while avoiding a substantial loss in signal for the high-J'' transition in the low temperature regions. To maintain temporally separated NO fluorescence signals, the laser pulses were separated in time by 250 ns.

For the OH temperature measurements, the lasers were tuned to the $P_1(7.5)$ and $Q_2(10.5)$ transitions, which were chosen to provide a higher temperature sensitivity ($\Delta\varepsilon_{12}/k \sim 2048$ K), as the OH was expected to exist only at temperatures above ~1000 K. Since the OH fluorescence lifetimes are short, a 100-ns laser separation was sufficient to temporally separate the fluorescence signals in these cases.

The respective fluorescence signals were imaged onto one of two intensified, cooled, charge-coupled device cameras (576×384 array with 23×23-μm pixels) equipped with uv f/4.5 lenses. In all cases, the imaged region was 30×45 mm, but the images have been trimmed to 20×45 mm for presentation. UG-5 and WG-305 Schott glass filters (2 mm thick) were used to block the laser scattering for the NO and OH measurements, respectively. The intensifier gate widths were set to provide ~200 ns and ~60 ns of uniform integration times for the NO and OH measurements, respectively. The laser pulses were carefully positioned (temporally) to occur just after the intensifier gates were fully on, to ensure uniform temporal integration of the fluorescence signals.

Data Reduction

The raw fluorescence images were corrected for camera dark background, flat field nonuniform response of the cameras and collection optics, laser energies and spatial distributions, and laser scattering. The laser sheet energy and its spatial profile were measured on a shot-to-shot basis using a dye-cell/video camera arrangement described elsewhere.[17,19] The flat field corrections for NO and OH were made using static cell in situ measurements of NO and acetone fluorescence, respectively.

When necessary during processing, one image was warped using a registration function (including translation, rotation, and magnification) to correct for the misalignment of the respective cameras. This correction was generally minor, though, because great care was taken to align the fields of view during the experiments to within 1–2 pixels throughout the images. The processed fluorescence images were software binned 2×2 to improve signal noise ratio, leading to a nominal resolution of approximately 300×160×160 μm. However, including the finite resolution of the imaging system and flow motion between laser pulses, the effective spatial resolution was ~0.3–0.5 mm.

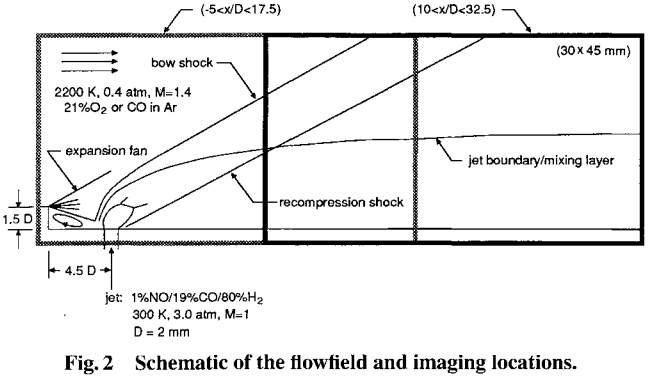

Fig. 2 Schematic of the flowfield and imaging locations.

Flowfield Description and Conditions

The flowfield examined here consists of a transverse jet in supersonic crossflow, with a single, sonic injector located downstream of a rearward facing step, as shown schematically in Fig. 2. Images were obtained within two (overlapping) regions, namely, $-5<x/D<17.5$ and $10<x/D<32.5$, with the jet located at $x/D=0$. The nominal flowfield conditions for these experiments are also shown in the figure. The temperatures and pressures listed are the static values of the freestream and the stagnation values of the jet reservoir. Although the freestream temperature used here (~2200 K) is higher than would be expected at the inlet of a scramjet combustor, it was chosen to reduce the autoignition time for the reacting cases, since no external ignition source was used in these experiments.

To simulate a scramjet flowfield, the jet was composed primarily of hydrogen, but also included 1% NO and 19% CO unless otherwise noted. In the NO measurements, the NO served as a fuel jet marker, whereas the CO acted to reduce the fluorescence lifetime of NO, thereby reducing the loss in spatial resolution due to flow motion.[19] In the OH measurements, the NO and CO effectively acted as diluents but were included to maintain the same fuel density in all cases. We should note that the addition of CO to the jet was found to enhance the mixing (see Results and Discussion), presumably due to a density ratio effect. This should be noted in any future comparison of these data with the pure hydrogen fuel case.

As indicated in Table 1, several freestream mixtures were used in these experiments. Argon was used as the freestream diluent in all cases to generate the desired postshock conditions. (The use of argon rather than nitrogen changes the freestream specific heat and density somewhat but is not expected to significantly affect the results of these experiments.) In the reacting experiments, the freestream contained 21% O_2 to simulate air. For the nonreacting NO measurements, 21% CO was used to provide an essentially nonoxidizing freestream with moderate quenching and identical flow conditions to the reacting case. (CO was used rather than nitrogen in the nonoxidizing freestream to reduce the fluorescence lifetime of NO in fuel lean regions, again to maintain spatial resolution.)

For these experiments, the jet-to-crossflow momentum ratio is ~1.9. The maximum jet Reynolds number [defined as $Re=(U_\infty-U_{jet})\delta/\nu$, where U_∞ and U_{jet} are the freestream and x-

Table 1 Freestream mixtures used for the OH and NO temperature measurements; for data set 4, the nominal freestream temperature includes heat release effects

Data set	Temperature tracer	Freestream mixture	Freestream temperature, K	Comments
1	NO	0.1%NO/21%CO/Ar	2160	Nonreacting; used for C_{12} calibration
2	NO	21%O_2/Ar	2160	Reacting
3	OH	21%O_2/Ar	2160	Reacting
4	OH	3%H_2/21%O_2/Ar	2190	Reacting; used for C_{12} calibration

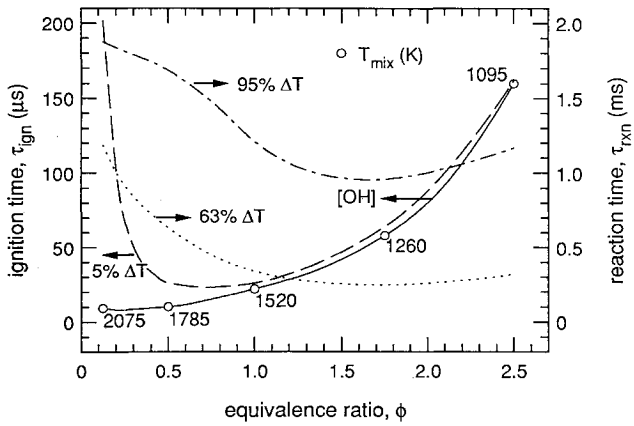

Fig. 3 Variation of ignition and heat release times as a function of equivalence ratio for $T_{jet} = 300$ K and $T_{\infty} = 2200$ K. Note the different scales for the ignition and heat release times; the labeled points indicate the mixture temperature at the given equivalence ratio.

component jet velocities, respectively, δ is the jet penetration, and ν is the average kinematic viscosity] is about 16,000 and occurs just downstream of the Mach disk. Based on this Reynolds number, the smallest temperature scales in the flow, which are on the order of the Batchelor scale ($\sim 25\delta Sc^{-1/2}Re^{-3/4}$, see, for example, Ref. 29), are approximately 90 μm. The resolution of these measurements is therefore 3–5 times more coarse than the smallest temperature scales in the flow. Although some smoothing of the steep temperature gradients and slight systematic temperature errors may occur due to inadequate spatial resolution,[9,19] the temperature measurements of the large-scale structures are not expected to be significantly affected.

Combustion and Heat Release Analysis

The extent of combustion and heat release expected within the imaged regions was estimated based on calculations performed using the Chemkin computer code[30] and a mechanism compiled by Mertens et al.[31] which includes H_2, O_2, NO, and CO chemistry. A simple one-dimensional enthalpy balance between the cold jet and the hot freesteam was used to model the variation of mixture temperature and equivalence ratio throughout the flowfield, assuming frozen chemistry.[19]

Representative results of this analysis are shown in Fig. 3. Two ignition criteria are shown, including the time at which a sharp rise in OH mole fraction is observed and the time at which 5% of the complete temperature rise is reached. Two heat release time scales are also shown (note the scale change in the figure), namely, the time required for the temperature to rise to 63 and 95% of its ultimate value. The points shown in the figure are for reference and indicate the initial mixture temperature at the corresponding equivalence ratio. Although not shown, the calculated temperature rise due to combustion ranges from ~100–1500 K, with the highest temperature increases occurring for the mixtures with the lowest initial temperatures.

Based on a maximum flow residence time of ~100 μs (assuming a plume velocity of ~0.6 mm/μs and $x/D < 32$), Fig. 3 suggests that OH formation due to autoignition is likely to occur within the imaged region, at least in the high-temperature, fuel-lean regions of this flowfield, i.e., the mixing/shear layer and near wall region. However, even with ignition in these regions, the time required for significant heat release (typically >300 μs for 63% of the final temperature rise) is much longer than the residence time of the flow within the image. Thus, no significant heat release is expected for these measurements.

We should note that although the calculations shown here include 1% NO and 19% CO in the fuel stream, no significant differences in ignition or heat release times were found in calculations for a pure hydrogen fuel jet. [As noted previously, NO can sensitize ignition, but the effect is most pronounced at high pressures and at mixture temperatures below ~1000 K (Ref. 20.)] In addition, these calculations show no significant consumption of NO for any of the conditions, during the time scales of interest in scramjet-type combustors (a few milliseconds). Hence, these results suggest that NO will act as a relatively stable fuel jet tracer in these flows and will not significantly perturb the combustion.

It is also worth noting that in these calculations the presence of O atoms was found to markedly reduce the (OH) ignition delay. In the flows considered here, this is not an issue because the O atom concentration is not appreciable, due to the relatively short test times. In previous studies,[8,32] however, the freestream O atom concentrations likely contributed to shorter ignition delays.

Results and Discussion

Simultaneous NO and OH Visualizations

Simultaneous NO and OH visualizations were obtained from both the upstream and downstream regions. In these measurements, the seeded NO marks the fuel jet fluid, whereas the OH, formed by the reaction of hydrogen in the jet with freestream oxygen, marks the reaction zones and convected combustion gases. Taken together, these measurements provide a means of characterizing the fuel penetration and locating the reaction zones, including the relative location of the reaction zone within the jet/freestream mixing layer. To obtain these visualizations, the first laser was tuned to the $Q_1(7.5)$ transition of OH, and the other laser was tuned to the $Q_1 + P_{21}(18.5)$ transition of NO. The lasers were fired sequentially with a delay of 100 ns and the resulting fluorescence signals were collected on different cameras.

Figure 4 shows examples of simultaneous NO and OH visualizations. Based on simple mixing and fluorescence signal analyses,[19] the OH signal in these images is expected to scale with OH concentration, with less than a ±25% deviation from a strictly linear relationship, primarily due to quenching variations. In contrast, a similar analysis indicates that the NO signal can only be qualitatively interpreted as the jet mole fraction, with the signal decreasing as the cold jet mixes with the warmer freestream, due to the fuel-NO dilution, increased quenching, and increased temperature.

As illustrated in these images, the OH within the plume is usually found first in diffuse pockets in the near wall ($y/D < 2$) region beyond $x/D \sim 8$. The fact that ignition occurs first in this region of the plume is likely the result of slower velocities in the lower wake region of the jet combined with the high temperatures and more ef-

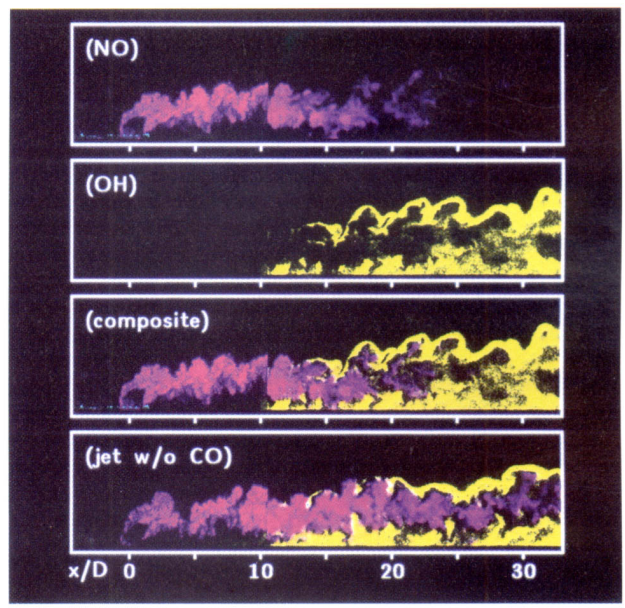

Fig. 4 Temporally resolved NO and OH visualizations. Each visualization is shown in a logarithmic color map (NO is violet, OH is yellow) and is a composite of two images covering $-5 < x/D < 10$ and $10 < x/D < 32.5$, respectively. Images a) and b) were obtained simultaneously in the same shock tube run with a jet compostion of 1%NO/19%CO/80%H_2. Image c) is a composite of image a) overlapped onto b). The composite image d) was obtained from a separate experiment with a jet composition of 1%NO/99%H_2.

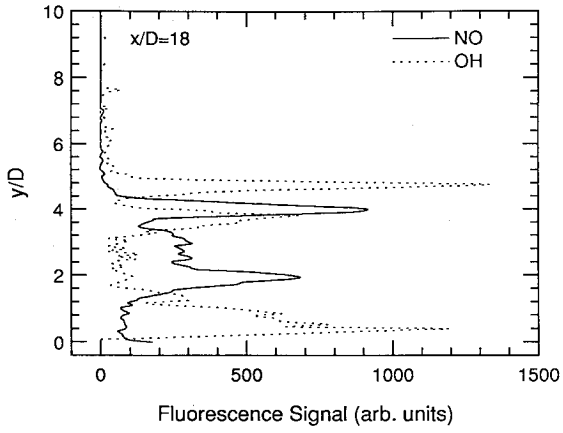

Fig. 5 NO and OH signal profiles for vertical cuts at $x/D = 18$ in the visualizations shown in Figs. 4a–4c; presence of OH at the outermost edge of the jet (surrounding an NO structure in this cut) suggests that the mixing-layer OH forms primarily in hot, fuel-lean regions.

ficient mixing (as indicated by the reduced NO signal). OH was also often observed in the recirculation zone just downstream of the step and, occasionally, weak OH signal was observed in spots along the upper edge of the jet for $x/D < 10$. Beyond $x/D = 10$, OH was observed in a relatively continuous filament in this mixing layer, much like that observed in previous investigations.[5,8,32]

In these visualizations, the NO signal generally decreases rapidly with downstream distance, which is indicative of the jet/freestream mixing. In examining Figs. 4c and 4d, we find a more rapid NO signal decrease in Fig. 4c, which indicates more rapid mixing for the case with 19% CO in the jet (Fig. 4c) compared to the case without (Fig. 4d). As noted previously, the enhanced mixing in Fig. 4c is believed to be due to a density ratio effect (i.e., a higher fuel density in Fig. 4c), because experiments substituting N_2 for CO showed the same effect, after correcting for the differences in quenching.

In Fig. 4, we also observe that the NO signal decreases sharply at the outer edge of the plume (indicating a sharp increase in temperature and/or a sharp decrease in jet fluid concentration), whereas the OH signal peaks on the edge of the plume (see Fig. 5). The large decrease in NO signal coupled with the appearance of strong OH signal on the outer edge of the plume suggests that the OH in the upper part of the plume forms on the hot (and lean) side of the jet boundary. Indeed, based on a detection sensitivity analysis of the NO signal, the equivalence ratio and temperature are estimated to be ~10% and ~2000 K at the location of peak OH signal (at $x/D = 18$). The presence of the OH here in the hot and lean shear layer region is consistent with the ignition calculations discussed earlier, and differs from a nonpremixed, turbulent jet flame, where the peak OH concentration is expected closer to the stoichiometric region.[33] Finally, we note that the images of Fig. 4 and the cuts in Fig. 5 illustrate the complementary nature of the OH and (jet-seeded) NO signals: where one is high, the other is low. With a large fraction of the measurement uncertainty due to signal-dependent shot noise, the accuracy of the temperature measurements will show a similar complementary nature.

Temperature Measurements

Temperature measurements of NO were obtained in the upstream region for both nonoxidizing and oxidizing freestreams. For the nonreacting NO measurements, the calculated temperature and the measured NO signal ratio in the freestream were used for in situ calibration of C_{12}. NO was not seeded into the oxidizing freestream in these experiments because of its propensity to oxidize during premixed storage. The lack of freestream NO combined with the lack of a reliable calibration location within the plume precluded in situ calibration in the oxidizing cases; hence, for these cases the average value of C_{12} from the nonreacting cases was used.

OH temperature measurements were obtained for cases with and without freestream OH (formed by autoignition of 3% H_2 added to the nominal 21% O_2/Ar freestream), at both the upstream and downstream imaged regions. Since little OH was observed for $x/D < 10$, the downstream measurements will be emphasized here. Similar to the NO measurements, the cases with freestream OH were calibrated in situ, and the resulting average C_{12} was used for the cases without freestream OH.

Based on previous verification measurements of NO[9] and OH[17] in simpler flows, we knew a priori of three small regions where the NO measurements would be unreliable: 1) within the barrel shock structure, 2) within the recirculation zone just downstream of the step, and 3) within the low pressure region just downstream of the barrel shock structure (approximately bounded by $0 < x/D < 1.5$, $0 < y/D < 1.5$). The NO temperatures are suspect in these regions because the fluorescence lifetimes were sufficiently long to cause signal from the first laser pulse to appear on the second image.

Instantaneous Temperature Fields/Comparisons

Figure 6 shows examples of temporally resolved NO and OH temperature images from reacting flow experiments. The NO measurements indicate that the temperature within the plume increases from ~300 K near the Mach disk to ~1200–1800 K at $x/D \sim 18$, due to the cool jet mixing with the warmer freestream. The near wall region ($y/D < \sim 2$) appears to mix most efficiently, reaching ~1000 K in just a few diameters. In contrast, the entrainment of freestream fluid into the plume core and upper plume region is somewhat less efficient, as evidenced by the pockets of relatively pure fuel (~500 K) which exist for 5–10 jet diameters.

As noted previously, OH is first observed within the plume in diffuse pockets in the near wall region at $x/D \sim 8$–10. The formation of OH at this location is consistent with the ignition calculations already discussed, based on the measured temperatures of 1500–2000 K and an approximate fuel residence time of 25–35 μs (assuming a plume velocity of ~0.6 mm/μs and $x/D \sim 8$–10). Farther downstream the OH eventually fills the entire plume due to both convection and chemical reaction. Within the plume core, the measured temperatures are somewhat cooler, with OH temperatures as low as 900–1000 K in some small pockets. Given the long ignition delays at low temperatures, these cooler OH pockets are likely due to warmer OH being entrained into cooler core fluid, on a time scale much faster than the relatively slow OH recombination time.

As shown in the image, the peak OH temperature in the upper mixing layer is ~2000 K, which, as already discussed, indicates that the OH forms on the lean side of the layer. The apparently longer delay in detectable concentrations of OH here compared to the near wall region may be due to a higher strain rate and/or a higher convective velocity. Although the peak temperatures measured in the mixing/shear layer reaction zone are reasonable, the layer may not be fully resolved because of the sharp gradients and limited spatial resolution (the OH layer is only a few times thicker than the spatial resolution of these measurements). Thus, the

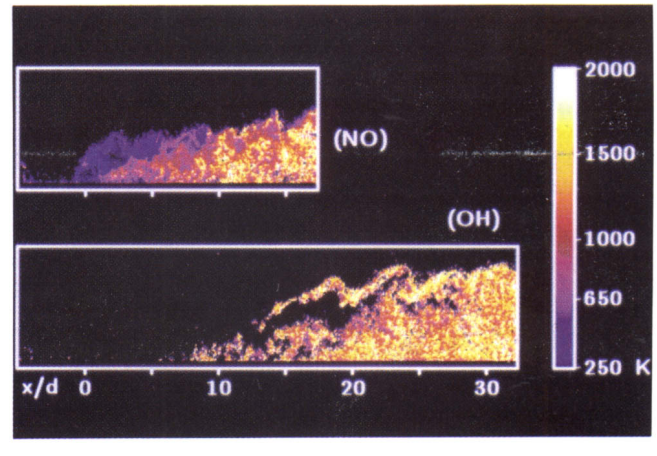

Fig. 6 Temporally resolved temperature measurements of NO and OH for an oxidizing freestream composed of 21% O_2 in argon.

cooler temperatures within the shear layer (as low as ~1000 K) are partly due to hot OH mixing with cooler core fluid and to the inability to resolve the sharp temperature gradients in the shear layer.

Despite the limited presence of OH in these images, we can make some comparisons with the NO measurements. For example, in the near wall region (for $10 < x/D < 18$) the OH and NO temperatures are in good agreement; both have spatially averaged values of ~1500 K and range from ~1000 to ~2000 K. Another interesting comparison can be made at the upper edge of the jet (near $x/D = 18$), where we find a higher peak temperature in the OH image (~2000 K compared to ~1500 K for NO). This apparent discrepancy is not a measurement error, but rather a consequence of the NO signal falling below the detectability limit in the hottest parts of the plume/shear layer interface.

The NO and OH temperature measurements also exhibit similar shot-to-shot uncertainties. For both, the primary sources of uncertainty are shot noise and fluctuations in the laser spectral profiles. For the NO measurements, we estimate that the shot-noise temperature uncertainty ranges from ~4–20% over the temperature range of 300–1500 K, and reaches as high as 40% at 1800 K due to the loss in signal from quenching by the freestream oxygen.[19] Within the plume, we estimate that the OH temperature uncertainty ranges from ~13–30%, with the variation primarily due to composition and quenching differences. Fluctuations in the value of C_{12}, which we attribute to laser spectral profile fluctuations,[9,17] were observed to be ~8 and ~9% for OH and NO, respectively. These fluctuations correspond to temperature uncertainties of 2–10% over 300–1800 K for NO, and 4–9% over 1000–2000 K for OH.

Frame-Averaged Temperature Fields/Comparisons

Although instantaneous temperature measurements highlight the large-scale structures, averages afford a better temperature comparison, because the fluctuations associated with the turbulent structures are removed. Figure 7 shows a comparison of frame-averaged NO and OH temperature fields for the reacting flow experiments. In this figure, the two average temperature fields are also shown spliced together in a composite image, using the NO measurements in the first half of the plume and the OH measurements in the second half. Each of these images was calculated by frame averaging a set of instantaneous temperature images (not the fluorescence images) and conditioning the average at each pixel on the presence of either NO or OH. We should note, however, that although these images show the general trends of the mean temperature distribution, the number of measurements included is not large enough to reach a fully converged average. This is evidenced by the remnants of turbulent structure in the shear layer region of each image.

In examining these images, many of the trends already noted for the instantaneous temperature images are observed in the averages

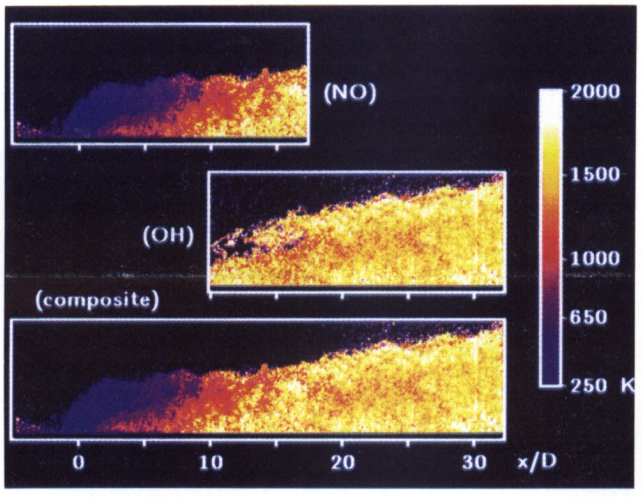

Fig. 7 Frame-averaged NO and OH temperature measurements: the NO image is a 6-frame average for the reacting flowfield condition, and the OH image is a 12-frame average at the same conditions; the lower image shows a composite of the two temperature fields, with OH data added to the end of the NO data.

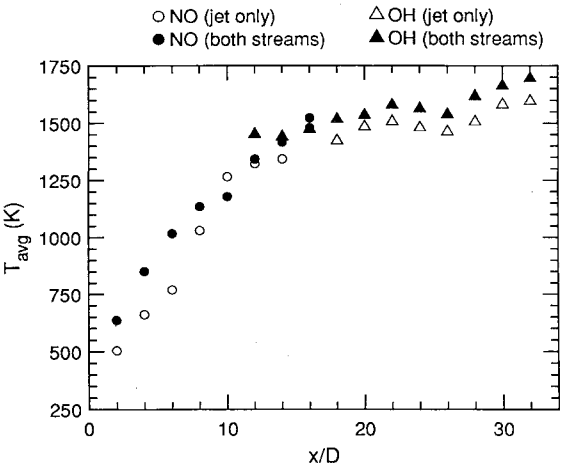

Fig. 8 Comparison of the average (measured) plume temperature as a function of axial distance for the four data sets; note the good agreement among the NO and OH temperatures.

as well. For example, in the NO image, the near wall region shows evidence of efficient mixing, with temperatures reaching more than ~1000 K within the first few diameters. Once again, the cooler temperatures in the upper plume region indicate less efficient mixing for $x/D < \sim 10$. As described earlier, the NO shear layer temperature appears somewhat cooler than that of the OH, because of the loss in detection sensitivity of NO in the hot, oxygen-rich mixing layer. Finally, in the OH image, we find that the plume core temperature measurements are incomplete because of the sparse and intermittent presence of OH for $x/D < 18$.

Given these exceptions, a simple visual inspection of the composite temperature image suggests that the NO and OH temperature measurements are in reasonably good agreement. Again, the only region where a direct comparison can be made is in the near wall region, with $0 < y/D < 2$ and $10 < x/D < 18$, because of the limited presence of OH in the overlapping images. In this region, the average NO and OH temperatures do agree well (~1500 K).

A more detailed comparison of the NO and OH temperature measurements is illustrated in Fig. 8, which shows the plume-averaged temperature as a function of axial distance. These temperatures were obtained by averaging the local mean plume temperatures in a 1-mm-wide vertical strip at each axial location. To improve the comparison, the average includes only pixel locations for which at least 80% of the instantaneous images contained fluorescence signals. This procedure primarily excludes the intermittent mixing layer region, i.e., approximately the upper 2–3 mm of the plume. In the figure, data are shown from all of the experiments in this study, including cases with and without freestream NO and OH. Compared in this way, we see that the difference between the NO and OH temperatures ranges between 2 and 7%, or ~25–100 K out of ~1400 K, in the common measurement region. The relatively good agreement between the NO and OH measurements here is noteworthy because it suggests the potential (J-dependent) systematic errors in the OH measurements are insignificant, having been minimized by calibration at high temperature.

In addition to showing the agreement among the measured NO and OH temperatures, these data also illustrate some measurement subtleties as well. For example, note that the (NO) measurements with NO in both streams show systematically higher temperatures than those with NO seeded only in the jet, particularly in the cool regions near the jet. The disparity in these measured temperatures does not represent a systematic error; it results from the different information each measurement provides. The measurements with NO in both streams largely indicate the mixed temperature, i.e., the combination of freestream and fuel (which may be stirred but not molecularly mixed), whereas the measurements with NO in only the jet indicate the fuel temperature. The fact that these two temperatures are different is an indication that the two streams are not molecularly mixed. Indeed, in the absence of complete molecular mixing, we expect the mixed temperature to be higher in these

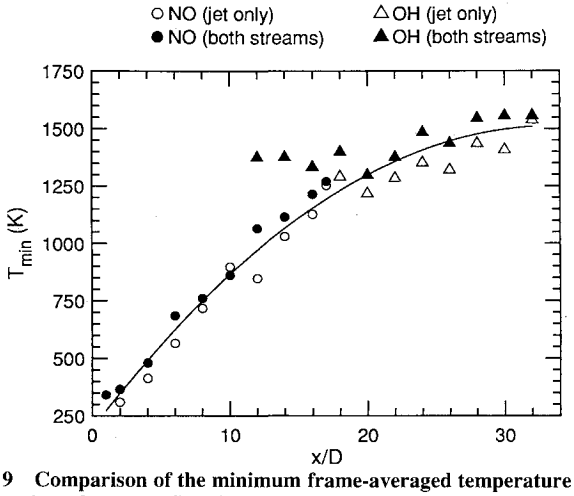

Fig. 9 Comparison of the minimum frame-averaged temperature for the various data sets; first four solid triangles illustrate a freestream temperature bias, since little fuel-generated OH is present in this region.

experiments, because the freestream fluid is generally warmer than the jet fluid. The difference, however, becomes less significant in the downstream regions, where entrainment and mixing has raised the fuel temperature closer to that of the freestream.

A similar effect can also occur for OH temperature measurements, although in the present experiments, to a lesser extent. The effect should be less significant for these OH measurements because the fuel-generated OH is only formed in hot regions of the plume ($T > 1200$ K), thereby reducing the temperature difference between fuel-generated and freestream OH. Although this effect may be partly responsible for the higher temperatures (see Fig. 8) measured with freestream OH, roughly 20 K of the observed disparity results from the slightly different freestream temperatures (see Table 1). Additionally, some of this observed temperature disparity could be due to a difference in fluorescence trapping for cases with and without freestream OH.

Another interesting comparison of the NO and OH temperature measurements is illustrated in Fig. 9, which shows the minimum (frame-averaged) plume temperature as a function of axial distance. In this figure, data have again been included from all of the experiments in this study, including cases with and without freestream NO and OH (the curve drawn through the data is shown to guide the reader's eye). The minimum temperature is relevant here in that it (ideally) marks the least-mixed jet fluid within the plume, as the cold jet mixes with the hot freestream; as a result, the distribution of the minimum plume temperature provides an indication of the rate of mixing at each axial location.[19]

Once again, we see that the temperatures for cases with freestream NO and OH show higher temperatures than the cases without, as we would expect based on the preceding discussion. We also observe that the minimum NO and OH temperatures agree within the scatter of the measurements, with the exception of the first four solid triangles. For these four data points, the OH temperatures are primarily based on entrained, freestream OH, since very little fuel-generated OH is present in this region. The fact that these points show warmer temperatures (than the NO measurements) is an indication that this entrained, freestream OH is not molecularly mixed with the fuel in the plume, resulting in the measured temperature being biased toward the freestream value. This biasing is an important effect to be aware of since it could potentially occur in other situations as well. In a supersonic combustion tunnel, for example, high temperature OH generated from upstream reaction zones may be entrained into cooler fuel-rich regions and bias the temperature measurements in a similar fashion.

Summary and Concluding Remarks

In this paper, we have described and compared results of two-line PLIF temperature measurements of NO and OH in a reacting scramjet model flowfield (300–2200 K). The respective temperature measurements were based on the sequential excitation of two transitions in the $A \leftarrow X$ (0,0) band of NO near 226 nm and the $A \leftarrow X$ (1,0) band of OH near 283 nm. Both temporally resolved and frame-averaged measurements of one or the other species were obtained through the use of two lasers and two cameras, with each camera integrating signal induced by only one of the lasers. In addition to the temperature results, simultaneous NO and OH visualizations were also presented, in which NO marked the fuel jet fluid and OH marked the reaction zones and entrained combustion gases.

With 1% NO seeded in the fuel, the NO signal levels were sufficient to obtain good quality temperature measurements throughout the (near field) plume, except for the lean shear layer reaction zone. Though not requiring seeding, the OH measurements provided less coverage of the flow, being limited to reaction zones and to regions containing some mixture of entrained or convected combustion gases, typically at temperatures above ~1000 K. In these experiments, the OH signal levels were comparable to those of NO because of the similar NO/OH concentrations (~0.1–1%), spectroscopic parameters, laser fluences, and effective quench rates within the common regions of the plume. Based on a comparison of the average temperature fields, the NO and OH temperatures in the common measurement regions agreed to within 2–7%, suggesting that no significant (J-dependent) systematic errors were observed for the OH measurements, when calibrated at high temperature (~2200 K).

In these experiments, the primary source of uncertainty is signal-dependent shot noise. The estimated instantaneous temperature uncertainties due to shot-noise ranged from 4–30% at our laser fluences of ~1 mJ/cm^2 and tracer concentrations of ~0.1–1%. Although these signal-dependent uncertainties are somewhat high, they could be easily reduced by a factor of 4 or more in future experiments by increasing the laser energy (by at least a factor of 5 without introducing significant nonlinear effects) and by using faster collection optics (e.g., f/2.5). The other major source of uncertainty in these measurements was shot-to-shot fluctuations in the laser spectral profiles, producing temperature uncertainties ranging from 2–10% for cases without in situ calibration.

The measurements presented here demonstrate that accurate NO and OH temperature measurements are feasible in supersonic combustion flows, but the measurements must be carefully interpreted, since they may be biased toward the fuel, freestream, or reaction zone temperatures, depending on the origin of the tracer and the degree of mixing. With careful interpretation, though, both techniques can provide powerful diagnostic tools for studying supersonic mixing and combustion flows.

Acknowledgments

This research was supported by the Air Force Office of Scientific Research, Aerospace Sciences Directorate, with Julian Tishkoff as Technical Monitor. The authors would like to acknowledge J. L. Palmer and A. L. Antonio for their assistance in carrying out these measurements, and M. F. Miller for many helpful discussions regarding this work.

References

[1]Clemens, N. T., Paul, P. H., Mungal, M. G., and Hanson, R. K., "Scalar Mixing in the Supersonic Shear Layer," AIAA Paper 91-1720, June 1991.

[2]Messersmith, N. L., and Dutton, J. C., "Laser Induced Fluorescence Measurements of Scalar Transport in Compressible Mixing Layers," AIAA Paper 92-3547, July 1992.

[3]Elliot, G., and Samimy, M., "Filtered Rayleigh Scattering Based Measurements in Compressible Mixing Layers," AIAA Paper 92-3543, July 1992.

[4]Miller, M., Island, T., Yip, B., Bowman, C., Mungal, M., and Hanson, R., "An Experimental Study of the Structure of a Compressible, Reacting Mixing Layer," AIAA Paper 93-0354, Jan. 1992.

[5]Lee, M. P., McMillin, B. K., Palmer, J. L., and Hanson, R. K., "Planar Fluorescence Imaging of a Transverse Jet in a Supersonic Crossflow," *Journal of Propulsion and Power*, Vol. 8, No. 4, 1992, pp. 729–735.

[6]Smith, M. W., and Northam, G. B., "Instantaneous Planar Visualization of Reacting Supersonic Flows Using Silane Seeding," AIAA Paper 91-1690, June 1991.

[7]Hollo, S. D., McDaniel, J. C., and Hartfield, R. J., Jr., "Characterization of Supersonic Mixing in a Nonreacting Mach 2 Combustor," AIAA Paper 92-0093, Jan. 1992.

[8]Parker, T. E., Allen, M. G., Foutter, R. R., Reinecke, W. G., Legner, H. H., Davis, S. J., and Rawlins, W. T., "An Experimental Study of Supersonic H_2-Air Combustion in a Shock Tunnel Flow Facility," *Twenty-Fourth Symposium (International) on Combustion*, Combustion Inst., Pittsburgh, PA, 1992, pp. 1613–1620.

[9]McMillin, B. K., Palmer, J. L., and Hanson, R. K., "Temporally Resolved, Two-Line Fluorescence Imaging of NO Temperature in a Transverse Jet in a Supersonic Crossflow," *Applied Optics*, Vol. 32, No. 36, 1993, pp. 7532–7545.

[10]Hanson, R. K., Seitzman, J. M., and Paul, P. H., "Planar Laser-Fluorescence Imaging of Combustion Gases," *Applied Physics B*, Vol. 50, No. 6, 1990, pp. 441–454.

[11]McMillin, B. K., Palmer, J. L., and Hanson, R. K., "Two-Dimensional Temperature Measurements of Shock Tube Flows Using Planar Laser-Induced Fluorescence Imaging of Nitric Oxide," AIAA Paper 91-1670, June 1991.

[12]Lee, M. P., McMillin, B. K., and Hanson, R. K., "Temperature Measurements in Gases Using Planar Laser-Induced Fluorescence Imaging of NO_2," *Applied Optics*, Vol. 32, No. 27, 1993, pp. 5379–5396.

[13]Palmer, J. L., McMillin, B. K., and Hanson, R. K., "Planar Laser-Induced Fluorescence Imaging of Velocity and Temperature in Shock Tunnel Free Jet Flow," AIAA Paper 92-0762, Jan. 1992.

[14]Cattolica, R. J., and Stephenson, D. A., "Two-Dimensional Imaging of Flame Temperature Using Laser-Induced Fluorescence," *Dynamics of Flames and Reactive Systems*, edited by J. R. Bowen, N. Manson, A. K. Oppenheim, and R. I. Soloukhin, Vol. 95, Progress in Aeronautics and Astronautics, AIAA, New York, 1984, pp. 714–721.

[15]Paul, P. H., Meier, U. E., and Hanson, R. K., "Single-shot, Multiple-Camera Planar Laser-Induced Fluorescence Imaging in Gaseous Flows," AIAA Paper 91-0459, Jan. 1991.

[16]Allen, M. G., Davis, S. J., and Donohue, K., "Planar Measurements of Instantaneous Species and Temperature Distributions in Reacting Flows: A Novel Approach to Ground Testing Instrumentation," AIAA Paper 90-2383, July 1990.

[17]Seitzman, J. M., Hanson, R. K., DeBarber, P. A., and Hess, C. F., "Application of Quantitative Two-Line OH Planar Laser-Induced Fluorescence for Temporally Resolved Planar Thermometry in Reacting Flows," *Applied Optics*, Vol. 33, No. 18, 1994, pp. 4000–4012.

[18]Laurendeau, N. M., "Temperature Measurements by Light-Scattering Methods," *Progress in Energy and Combustion Science*, Vol. 14, No. 2, 1988, pp. 147–170.

[19]McMillin, B. K., "Instantaneous Two-Line PLIF Temperature Imaging of Nitric Oxide in Supersonic Mixing and Combustion Flowfields," Ph.D. Thesis, Dept. of Mechanical Engineering, Stanford Univ., Stanford, CA, May 1993.

[20]Slack, M., and Grillo, A., "Investigation of Hydrogen-Air Ignition Sensitized by Nitric Oxide and Nitrogen Dioxide," NASA CR-2896, Oct. 1977.

[21]Chang, A. Y., Di Rosa, M. D., and Hanson, R. K., "Temperature Dependence of Collision Broadening and Shift in the NO $A \leftarrow X$ (0,0) Band in the Presence of Argon and Nitrogen," *Journal of Quantitative Spectroscopy and Radiative Transfer*, Vol. 47, No. 5, 1992, pp. 375–390.

[22]McDermid, I. S., and Laudenslager, J. B., "Radiative Lifetimes and Electronic Quenching Rate Constants for Single-Photon-Excited Rotational Levels of NO ($A^2\Sigma^+, v' = 0$)," *Journal of Quantitative Spectroscopy and Radiative Transfer*, Vol. 27, No. 5, 1982, pp. 483–492.

[23]McGee, T. J., Miller, G. E., Burris, J., Jr., and McIlrath, T. J., "Fluorescence Branching Ratios From the $A^2\Sigma^+(v' = 0)$ State of NO," *Journal of Quantitative Spectroscopy and Radiative Transfer*, Vol. 29, No. 4, 1983, pp. 333–338.

[24]Nutt, G. F., Haydon, S. C., and McIntosh, A. I., "Measurement of Electronic Quenching Rates in Nitric Oxide Using Two-Photon Spectroscopy," *Chemical Physics Letters*, Vol. 62, No. 2, 1979, pp. 402–404.

[25]Seitzman, J. M., and Hanson, R. K., "A Comparison of Excitation Techniques for Quantitative Fluorescence Imaging of Reacting Flows," *AIAA Journal*, Vol. 31, No. 3, 1993, pp. 513–519.

[26]Rea, E. C., Chang, A. Y., and Hanson, R. K., "Collisional Broadening of the $A^2\Sigma^+ \leftarrow X^2\Pi$ (0,0) Band of OH by H_2O and CO_2 in Atmospheric-Pressure Flames," *Journal of Quantitative Spectroscopy and Radiative Transfer*, Vol. 41, No. 1, 1989, pp. 29–42.

[27]Copeland, R. A., Wise, M. L., and Crosley, D. R., "Vibrational Energy Transfer and Quenching of OH ($A^2\Sigma^+, v' = 1$)," *Journal of Physical Chemistry*, Vol. 92, No. 20, 1988, pp. 5710–5715.

[28]Quagliaroli, T. M., Laufer, G., Krauss, R. H., and McDaniel, J. C., Jr., "Laser Selection Criteria for OH Fluorescence Measurements in Supersonic Combustion Test Facilities," *AIAA Journal*, Vol. 31, No. 3, 1993, pp. 520–527.

[29]Dowling, D. R., and Dimotakis, P. E., "Similarity of the Concentration Field of Gas-Phase Turbulent Jets," *Journal of Fluid Mechanics*, Vol. 218, Sept. 1990, pp. 109–142.

[30]Kee, R. J., Rupley, F. M., and Miller, J. A., "Chemkin-II: A Fortran Chemical Kinetics Package for the Analysis of Gas-Phase Chemical Kinetics," Sandia National Lab. Rept. SAND89-8009, Livermore, CA, 1989; and "The Chemkin Thermodynamic Data Base," Sandia National Labs. Rept. SAND87-8215B, Livermore, CA, 1990.

[31]Mertens, J. D., Chang, A. Y., Hanson, R. K., and Bowman, C. T., "A Shock Tube Study of Reactions of Atomic Oxygen with Isocyanic Acid," *International Journal of Chemical Kinetics*, Vol. 24, No. 3, 1992, pp. 279–295.

[32]Rothstein, A. D., and Wantuck, P. J., "A Study of the Normal Injection of Hydrogen Into a Heated Supersonic Flow Using Planar Laser-Induced Fluorescence," AIAA Paper 92-3423, July 1992.

[33]Barlow, R. S., Dibble, R. W., Chen, J.-Y., and Lucht, R. P., "Effect of Damkohler Number on Superequilibrium OH Concentration in Turbulent Nonpremixed Jet Flames," *Combustion and Flame*, Vol. 82, No. 2, 1990, pp. 235–251.